IVYSPRING INTERNATIONAL PUBLISHER

Theranostics

2019; 9(10): 2924-2938. doi: 10.7150/thno.35274

Research Paper

Development and characterization of a theranostic multimodal anti-PSMA targeting agent for imaging, surgical guidance, and targeted photodynamic therapy of PSMA-expressing tumors

Susanne Lütje[1,2,4], Sandra Heskamp[1], Gerben M. Franssen[1], Cathelijne Frielink[1], Annemarie Kip[1], Marlène Hekman[1], Giulio Fracasso[3], Marco Colombatti[3], Ken Herrmann[2], Otto C. Boerman[1], Martin Gotthardt[1], Mark Rijpkema[1] ✉

1. Department of Radiology and Nuclear Medicine, Radboud university medical center, Nijmegen, the Netherlands
2. Clinic for Nuclear Medicine, University Hospital Essen, Germany
3. Department of Medicine, University of Verona, Verona, Italy
4. Department of Nuclear Medicine, University Hospital Bonn, Bonn, Germany

✉ Corresponding author: Mark Rijpkema, PhD. Department of Radiology and Nuclear Medicine, Radboud university medical center, Geert Grooteplein Zuid 10, 6525 GA Nijmegen, The Netherlands. Phone: +31 24 36 14511 email: Mark.Rijpkema@radboudumc.nl

Received: 2019.03.27; Accepted: 2019.03.29; Published: 2019.05.04

Abstract

Rationale: Prostate cancer (PCa) recurrences after surgery frequently occur. To improve the outcome after surgical resection of the tumor, the theranostic multimodal anti-PSMA targeting agent ^{111}In-DTPA-D2B-IRDye700DX was developed and characterized for both pre- and intra-operative tumor localization and eradication of (residual) tumor tissue by PSMA-targeted photodynamic therapy (tPDT), which is a highly selective cancer treatment based on targeting molecules conjugated to photosensitizers that can induce cell destruction upon exposure to near-infrared (NIR) light.

Methods: The anti-PSMA monoclonal antibody D2B was conjugated with IRDye700DX and DTPA and subsequently radiolabeled with ^{111}In. To determine the optimal dose and time point for tPDT, BALB/c nude mice with PSMA-expressing (PSMA$^+$) s.c. LS174T-PSMA xenografts received the conjugate (24-240 µg/mouse) intravenously (8 MBq/mouse) followed by µSPECT/CT, near-infrared fluorescence imaging, and ex vivo biodistribution at 24, 48, 72 and 168 h p.i. Tumor growth of LS174T-PSMA xenografts and overall survival of mice treated with 1-3 times of NIR light irradiation (50, 100, 150 J/cm^2) 24 h after injection of 80 µg of DTPA-D2B-IRDye700DX was compared to control conditions.

Results: Highest specific tumor uptake was observed at conjugate doses of 80 µg/mouse. Biodistribution revealed no significant difference in tumor uptake in mice at 24, 48, 72 and 168 h p.i. PSMA$^+$ tumors were clearly visualized with both µSPECT/CT and NIR fluorescence imaging. Overall survival in mice treated with 80 µg of DTPA-D2B-IRDye700DX and 1x 150 J/cm^2 of NIR light at 24 h p.i. was significantly improved compared to the control group receiving neither conjugate nor NIR light (73 days vs. 16 days, respectively, p=0.0453). Treatment with 3x 150 J/cm^2 resulted in significantly prolonged survival compared to treatment with 3x 100 J/cm^2 (p = 0.0067) and 3x 50 J/cm^2 (p = 0.0338).

Principal conclusions: ^{111}In-DTPA-D2B-IRDye700DX can be used for pre- and intra-operative detection of PSMA$^+$ tumors with radionuclide and NIR fluorescence imaging and PSMA-targeted PDT. PSMA-tPDT using this multimodal agent resulted in significant prolongation of survival and shows great potential for treatment of (metastasized) prostate cancer.

Key words: PSMA, prostate cancer, targeted photodynamic therapy, intra-operative, near-infrared fluorescence

Introduction

Despite improvements in diagnosis and therapy, prostate cancer (PCa) remains a significant health problem with 180,890 estimated new cases and 26,120 estimated deaths in the US in 2016 [1]. At present, the curative treatment option for localized stages of PCa is radical prostatectomy, which may include extended lymph node dissection in case of intermediate- and high-risk localized PCa [2, 3]. Unfortunately, two main factors limit the success of surgical procedures: First, translation of pre-operatively obtained images to the surgical field can be challenging, increasing the risk for smaller tumor lesions to be missed by the surgeon. Secondly, wide local excision of tumor lesions in the lower pelvis may be precluded due to close proximity of the lesions to important healthy structures such as urinary bladder wall or erectile nerves, leading to positive surgical margins after radical prostatectomy in 11-48% of patients [4-6]. In both cases, lesions may grow out to cause recurrence of the disease.

Photodynamic therapy is an ablative procedure, in which tumor cells can be destroyed efficiently by irradiation of light of a specific wavelength, which activates a previously administered photosensitizer (PS). Upon absorption of photons, the PS is activated and undergoes photochemical reactions producing reactive oxygen species (ROS) by transfer of energy from the PS to the oxygen present in the tissue. Consequently, the produced ROS such as hydroxyl radicals, hydrogen peroxide, and superoxide can cause cellular damage. Clinical studies revealed that photodynamic therapy can be curative, particularly in early stage tumors [7]. In addition, the survival in patients with inoperable cancers can be prolonged. Even though the principle of photodynamic therapy has been known for several decades, it has not been fully exploited for clinical uses, yet. The major reasons that restrict full clinical exploitation of conventional PDT are insufficient delivery of the photosensitizer to tumor tissue, resulting in a limited anti-tumor effect. Moreover, especially in the non-targeted approach, accumulation of the photosensitizer into healthy tissues could result in adverse effects such as phototoxic and photoallergic reactions.

To overcome these obstacles, a targeted approach of photodynamic therapy has been developed. In this so-called targeted photodynamic therapy (tPDT), selectivity is enhanced by conjugation of the photosensitizer to a tumor targeting vehicle thereby allowing selective and effective treatment of tumor remnants [8]. The prostate-specific membrane antigen (PSMA) is an integral membrane glycoprotein which is overexpressed in the majority of PCa [9]. Due to its selective overexpression in 90-100% of local PCa lesions, malignant lymph nodes, and bone metastases [10-12], PSMA has been recognized as an ideal target for imaging and therapy of PCa [13-17].

To address the issue of intra-operative tumor localization and eradication of residual tumor tissue to improve treatment of PCa, we developed a theranostic approach using the anti-PSMA mAb D2B labeled with ^{111}In and conjugated to the photosensitizer IRDye700DX. This multimodal PSMA-targeting agent can be used for theranostic applications: First, the extent of the tumor can be estimated pre-operatively by SPECT/CT. Second, the radiosignal may be used for surgical guidance using a gamma probe during surgery. Third, the fluorescence signal of the photosensitizer IRDye700DX may be used for intra-operative visualization of tumor tissue with near-infrared fluorescence (NIRF) imaging, to guide resection of the tumor and to mark potential areas with tumor remnants for tPDT. Finally, our theranostic agent allows intra-operative tPDT for tumor-specific destruction of residual tumor tissue that could not be removed surgically, for instance in the lower pelvis where proximity of the prostate to rectum, sphincter and erectile nerves precludes wide local excision.

Materials and Methods

Reagents

The mAb D2B (IgG1) was derived from mice that were immunized three times with a cell lysate of membranes of LNCaP cells [18-20]. Mice were also boosted with a recombinant form of PSMA produced in bacteria. D2B IgG was purified from hybridoma culture supernatant by Protein A affinity chromatography [18, 20]. IRDye700DX NHS ester was purchased from LI-COR Biosciences (Lincoln, NE).

Synthesis of IRDye700DX-D2B-DTPA

170 µl of 1 M $NaHCO_3$, pH 8.5 was added to D2B IgG (5 mg in 1700 µl PBS, 32 nmol) for conjugation of D2B with N-hydroxysuccinimide (NHS)-IRDye700DX (LI-COR Biosciences) in DMSO, with a 10-fold molar excess of NHS-IRDye700DX (650 µg, 333 nmol). After 1 h of incubation at room temperature on an orbital shaker in the dark, 650 µg (1000 nmol) of p-isothiocyanatobenzyl-diethylene-triamine-penta-acetic acid (ITC-DTPA) (Macrocyclics, Dallas, TX) in DMSO was added to the reaction mix in 190 µl of 1 M $NaHCO_3$, pH 9.5, in a 31-fold molar excess, which under such circumstances commonly leads to a

substitution rate around 3 [21]. DTPA was conjugated to the lysine residues of the antibody. After 1 h of incubation at room temperature on an orbital shaker in the dark, the reaction mixture was dialyzed for 3 days in a Slide-A-Lyzer (10-kDa cutoff, Thermo Scientific, Schwerte, Germany) against 0.25 M NH_4Ac, pH 5.4. The dialysis buffer was replaced 2x per day during the 3-day dialysis period. The photosensitizer-to-antibody substitution ratio of the purified conjugate was determined with an Ultrospec 2000 spectrophotometer (Pharmacia Biotech, Freiburg, Germany) at wavelengths of 280 nm and 689 nm and was calculated using the formula: substitution ratio = $0.875*E_{689}/(E_{280}-(0.03*E_{689}))$. The 0.875 represents the ratio between the extinction coefficient at 280 and 689 nm, and 0.03 is an estimation for IRDye700DX signal contributing to the absorption, as indicated by the manufacturer. The molar substitution ratio of the conjugate (700DX-D2B) used in these studies was 3.3.

Radiolabeling of IRDye700DX-D2B-DTPA

For *in vitro* studies, 25 µg of IRDye700DX-D2B-DTPA was radiolabeled with 25 MBq ^{111}In (Mallinckrodt, Petten, the Netherlands) in 0.5 M MES buffer pH 5.4 (three times the volume of ^{111}In-chloride) and incubated during 30 min at room temperature under metal-free conditions. Following incubation, 50 mM EDTA was added to the final concentration of 5 mM to chelate unincorporated ^{111}In. The labeling efficiency was determined by instant thin layer chromatography (ITLC) using 0.1 M citrate buffer, pH 6.0, as the mobile phase. Labeling efficiency was 86%, and after PD10 purification radiochemical purity exceeded 95%.

For the protein dose escalation and time optimization study (24, 80, and 240 µg/mouse), 150, 450, and 1200 µg of IRDye700DX-D2B-DTPA was radiolabeled with 50 MBq ^{111}In. The labeling efficiency was 81, 93, and 96 % for the 24, 80, and 240 µg group, respectively. ^{111}In-DTPA-D2B-IRDye700DX was purified by gel filtration on a PD-10 column, and the radiochemical purity of the final dual-labeled tracer was ≥ 97%, as determined by ITLC.

Serum stability

Samples of commercial mouse serum purchased from Bodinco B.V. (Alkmaar, the Netherlands) were used to determine the *in vitro* serum stability of ^{111}In-DTPA-D2B-IRDye700DX (10 µg D2B, 0.37 MBq/µg) by ITLC using 0.1 M citrate buffer, pH 6.0, as the mobile phase. Stability was evaluated at 0, 0.5, 2.5, 6, and 24 h incubation at 37 ºC. In addition, fluorescence intensity at each of these time points was measured on a TECAN infinite M200 Pro in serum and PBS in triplicate. Fluorescence intensity at t=0 was set to 100% and all other time points were analyzed in correlation to t=0.

Cell culture

The PSMA-transfected colon carcinoma cell line LS174T-PSMA was cultured in RPMI 1640 medium, supplemented with 10% fetal calf serum (Life technologies, Carlsbad, CA) and 2 mM of glutamine in the presence of 0.3 mg/mL G418 geneticin [20]. PSMA-negative LS174T-wildtype colon carcinoma cells were cultured in RPMI 1640 medium, supplemented with 10% fetal calf serum and 2 mM of glutamine.

Immunoreactivity

The immunoreactive fraction of the dual-labeled ^{111}In-DTPA-D2B-IRDye700DX was compared to that of ^{111}In-DTPA-D2B using freshly trypsinized LS174T-PSMA cells in triplicate, essentially as described by Lindmo et al [22]. Briefly, a serial dilution of LS174T-PSMA cells (6.6×10^5 to 2.1×10^7 cells/mL) in 0.5 mL RPMI medium containing 0.5% BSA was incubated at 37 °C for 1 h with 0.1 pmol ^{111}In-DTPA-D2B-IRDye700DX (250 Bq). An excess of unlabeled DTPA-D2B-IRDye700DX (1,300 pmol) was added to a duplicate of the lowest cell concentration to determine nonspecific binding [20]. After incubation, cells were spun down and the pellet was washed with binding buffer (500 µL RPMI medium containing 0.5% BSA). The activity in the vials and in the cell pellet was determined in the gamma counter (2480 WIZARD^2 Automatic Gamma Counter, PerkinElmer). The inverse of the specific cell bound activity was plotted against the inverse of the cell concentration, and the immunoreactive fraction was calculated from the y-axis intercept using GraphPad Prism software (version 5.03 for Windows; GraphPad Software, La Jolla, USA) [20].

Internalization capacity

LS174T-PSMA cells were cultured in six-well plates to confluency and were incubated with 1.9 kBq of ^{111}In-DTPA-D2B (3.2-3.5 ng/well) or ^{111}In-DTPA-D2B-IRDye700DX (2.6-2.7 ng/well) for 2, 4, 24, and 48 h in 2 mL binding buffer (RPMI + 0.5% BSA) at 37 °C in a humidified atmosphere with 5% CO_2. Nonspecific binding was determined by coincubation with unlabeled D2B (5 µg/well). After incubation, acid wash buffer (0.1 M HAc, 0.15 M NaCl, pH2.6) was added for 10 min to remove the membrane-bound fraction of the cell-associated ^{111}In-labeled compounds. Subsequently, cells were harvested from the six-well plates and the amount of membrane-bound and internalized activity was measured in a gamma counter.

Competitive binding assay

The 50% inhibitory concentration (IC_{50}) of D2B IgG and DTPA-D2B-IRDye700DX was determined as described previously using PSMA-expressing LS174T-PSMA cells in a competitive binding assay with ^{111}In-labeled D2B as a tracer [19, 20, 23]. The LS174T-PSMA cells were grown in 6-well plates to confluency, followed by incubation on ice for 2 h in 1 mL of binding buffer with 1.9 kBq of ^{111}In-labeled D2B IgG (2.6 ng) and a series of increasing concentrations (0.005-300 nM) of unlabeled D2B IgG [19, 20]. After incubation, cells were washed with binding buffer and the cell-associated activity was measured in a gamma-counter [19, 20]. The IC_{50} values were calculated using GraphPad Prism software.

PSMA-targeted photodynamic therapy *in vitro*

PSMA$^+$ LS174T-PSMA and PSMA$^-$ LS174T cells were seeded into transparent 48-well plates (Thermo Scientific) (150,000 cells/well) and incubated for 48 h in RPMI 1640 medium, supplemented with 10% fetal calf serum and 2 mM of glutamine in the presence of 0.3 mg/mL G418 geneticin. On the day of the experiment, cells were washed once with PBS and medium was replaced by 10 µg/mL of the DTPA-D2B-IRDye700DX conjugate in RPMI (250 µl volume per well). As negative control for NIR light irradiation effects, cells were included that only received PBS without DTPA-D2B-IRDye700DX. After incubation for 1 h at 37 °C, cells were washed with PBS and 500 µl of RPMI medium was added to the cells. Subsequently, cells were irradiated with a NIR light–emitting diode that emits light at a wavelength of 670 to 710 nm [24]. The typical forward voltage was 2.6 V creating a power output of 490 mW using 126 individual LED bulbs to ensure homogenous illumination of the area of interest predefined as 5 x 3 cm. The cells were irradiated at NIR radiant exposures of 2, 5, 10, 30, 50, 100, and 150 J/cm^2. All *in vitro* experiments were carried out in triplicate. As control for cellular toxicity of the DTPA-D2B-IRDye700DX conjugate, cells incubated with DTPA-D2B-IRDye700DX that were not irradiated with NIR light were included.

Analysis of phototoxicity *in vitro*

Cytotoxic effects of photodynamic therapy with D2B-IRDye700DX were determined with a CellTiter-Glo™ assay (Promega Benelux, Leiden, the Netherlands) according to the instructions of the manufacturer at 1 h after irradiation. Briefly, all cells were incubated for 1 h under light-protected conditions at room temperature. Subsequently, medium was replaced by 100 µl of RPMI and 100 µl of the CellTiter-Glo™ reagent was added [25]. The 48-well plates were shaken for 2 min and incubated for 10 min at room temperature. Of each well, 100 µl was transferred to a black flat-bottom 96-well plate. The intensity of the luminescent signal associated to the amount of ATP present in the cell lysates was measured on a TECAN infinite M200 Pro. Cell viability of control cells was set to 100% and cell viability of treated cells (NIR light + conjugate) was calculated in relation to this value.

Animal tumor model

Male BALB/c nude mice (Janvier, Le Genest Saint Isle, France), 8-10 weeks old, were housed in individually ventilated cages (5 mice per cage) under nonsterile standard conditions with free access to chlorophyll-free animal chow (Ssniff, Soest, the Netherlands) and water. Mice were subcutaneously inoculated with 2.5 x 10^6 PSMA$^+$ LS174T-PSMA cells or PSMA$^-$ LS174T-wildtype cells in 200 µL of complete RPMI 1640 medium in the right flank. Xenografts grew to approximately 0.1 g in 7 days after tumor cell inoculation [20]. All experiments have been approved by the Central Committee on Animal Experimentation and institutional Animal Welfare Committee of the Radboud University Medical Center and were conducted in accordance to the guidelines of the Revised Dutch Act on Animal Experimentation. Humane endpoints were: tumor size, ulceration or invasive tumor growth, abnormal mobility due to tumor growth, other signs of severe clinical discomfort (dehydration, 15% weight loss in less than 2 days).

Dual-modality µSPECT/CT and NIRF imaging and biodistribution

Male BALB/c nude mice (5 mice per group) with s.c. PSMA-expressing LS174T-PSMA tumors received 30 µg of ^{111}In-DTPA-D2B-IRDye700DX (5-8 MBq/mouse), intravenously. All mice were imaged on both an IVIS fluorescence imaging system (Xenogen VivoVision IVIS Lumina II, Caliper Life Sciences, Lincolnshire, UK) with an acquisition time of 10 s, and a small-animal µSPECT/CT scanner (U-SPECT II, MILabs, Utrecht, the Netherlands) with a 1.0 diameter pinhole collimator tube (acquisition time: 15 min, 20 min, 26 min and 65 min at 24, 48, 72, and 168 h p.i., respectively) under inhalation anesthesia with isoflurane, followed by a CT scan (spatial resolution 160 µm, 65 kV, 615 µA) for anatomical reference. Scans were reconstructed with MILabs reconstruction software, using an ordered-subset expectation maximization algorithm, energy window 154 - 188 keV, 3 iterations, 16 subsets, and voxel size of 0.2 mm. SPECT/CT scans were analyzed and maximum intensity projections (MIPs)

were created using the Inveon Research Workplace software (IRW, version 4.1). NIRF images were analyzed using Living Image software version 4.2. To determine the time point at which the highest tumor accumulation of ^{111}In-DTPA-D2B-IRDye700DX was reached, at 24, 48, 72, and 168 h p.i. 5 mice were euthanized with CO_2/O_2 asphyxiation after scanning. Tissues of interest (tumor, muscle, lung, spleen, liver, kidneys, stomach, pancreas, duodenum, and prostate) were dissected, weighed and measured for radioactivity in a gamma counter (2480 WIZARD^2 Automatic Gamma Counter, PerkinElmer), as described previously [19, 20, 26]. Blood samples were obtained by heart puncture. An aliquot of the injected dose was counted simultaneously on the gamma counter to allow calculation of the uptake of radioactivity in each tissue as a fraction of the injected dose.

In a biodistribution study, male BALB/c nude mice (5 mice per group) with s.c. PSMA-expressing LS174T-PSMA tumors received 24, 80, or 240 µg of ^{111}In-DTPA-D2B-IRDye700DX (8 MBq/mouse), intravenously. At 24 h after injection, all mice were imaged on both an IVIS fluorescence imaging system and a µSPECT/CT scanner as described above, followed by euthanasia with CO_2/O_2 asphyxiation. Tissues of interest (tumor, muscle, lung, spleen, liver, kidneys, stomach, pancreas, duodenum, and prostate) were dissected, weighed and measured for radioactivity in a gamma counter as described above.

PSMA-targeted photodynamic therapy *in vivo*

Mice with s.c. PSMA$^+$ LS174T-PSMA tumors were block randomized into 6 groups of 7 animals based on tumor size at 7 days after inoculation of the tumor cells. Mice received 80 µg of DTPA-D2B-IRDye700DX intravenously via the tail vein followed by exposure to different NIR light irradiation regimens at 24h after injection of the conjugate. For NIR light irradiation, mice were placed under the NIR light–emitting diode that emits light at a wavelength of 670 to 710 nm [24]. The typical forward voltage was 2.6 V creating a power output of 490 mW using 126 individual LED bulbs to ensure homogenous illumination of the area of interest predefined as 5 x 3 cm. The distance from diode to skin surface was 5 cm. Seven mice did not receive the tracer and were not irradiated (control group).

Previously, unconjugated D2B was shown to have no therapeutic efficacy [27]. To determine the therapeutic effect of D2B-IRDye700DX itself DTPA-D2B-IRDye700DX was tested in mice that did not receive irradiation after administration of the conjugate. This condition was compared to mice that did not receive the conjugate but did receive NIR light irradiation and to mice that received neither conjugate nor NIR light irradiation. In addition, mice with s.c. PSMA-negative LS174T-wildtype tumors were included as negative control. These mice received 80 µg of DTPA-D2B-IRDye700DX intravenously followed by exposure to different NIR light irradiation regimens at 24h after injection of the conjugate.

To determine the treatment efficacy, the diameter of the tumors was measured twice a week in three dimensions with an external caliper by the same person for all measurements. This person was blinded for group stratification. Tumor volumes were calculated using the following formula: (length x width x depth)/2. Mice were observed daily, and were euthanized by CO_2/O_2 asphyxiation when tumor volume reached more than 1000 mm^3. In addition, mice were removed from the experiment humane endpoints were reached, scored by a blinded biotechnician. Overall survival was defined as the day when tumors reached a size of 1000 mm^3 or at which humane endpoints were reached. Progression-free survival was defined as the time point after NIR light exposure at which tumors showed progression in size after a period of regression/stable disease. Blood samples of 0.1 mL were collected via submandibular bleeding before and after therapy to determine blood creatinine and liver enzymes (ASAT, ALAT) to evaluate nephro- and hepatotoxicity, respectively.

Immunohistochemistry

LS174T-PSMA tumors from mice treated with tPDT (5 mice per time point) at a NIR radiant exposure of 150 J/cm^2 or from untreated control mice (5 mice) were harvested at 1 h or 24 h after NIR light irradiation and fixated in 4% buffered formalin. Tissues were subsequently embedded in paraffin and sectioned at 4 µm thickness. Tissue sections were stained with hematoxylin and eosin (H&E) to visualize morphology. An immunohistochemical protocol was followed to stain the tissue sections with either anti-Ki-67 antibody (1:100 dilution, rabbit monoclonal, Thermo Scientific), anti-caspase-3 antibody (1:4000 dilution, rabbit anti human/mouse cleaved caspase-3, Cell Signaling) or anti-γH2AX antibody (1:1000 dilution, rabbit anti H2AX, Cell Signaling). Briefly, slides were deparaffinized by xylene wash and rehydrated using ethanol. Antigen retrieval was performed with 10 mM citrate pH 6.0 in PT-Module (10 min, 96 °C). Endogenous peroxidase activity was quenched with 3% H_2O_2 for 10 min. After preincubation with 20% normal goat serum for 30 min, the slides were incubated with rabbit anti anti-caspase antibody (1:4000) respectively rabbit anti H2AX (1:1000) in a humidified chamber at 4°C

overnight in the dark. After preincubation with 20% normal swine serum, the slides were incubated with rabbit anti Ki-67 (1:100) for 60 min at room temperature. Subsequently, the slides were washed 3 times with 10 mM PBS. The slides stained with caspase-3 and H2AX were incubated with goat-anti-rabbit-biotin (1:200 Vector Laboratories) for 30 min at RT after washing with PBS followed by the incubation with Vectastain Elite ABC kit (Vector Laboratories) for 30 min. The slides stained with Ki-67 were incubated with the secondary antibody swine-anti-rabbit-peroxidase (1:200, DAKO) After washing with PBS, the bound antibodies were visualized using diaminobenzine (DAB, Sigma-Aldrich). All slides were counterstained with 3 times diluted hematoxylin (Klinipath) for 5 seconds and mounted with a cover slip (permount, Fisher Scientific).

Immunohistochemical stainings were analyzed by two observers (CF and SL) in consensus and categorized using an ordinal 5-point scale ranging from 0 (no staining), 1 (weak staining), 2 (intermediate staining), 3 (intense staining) to 4 (very intense staining). In total, the observers scored 5 NIR treated tumors per time point (1 vs. 24 h post irradiation) and per staining (caspase-3, yH2AX, and Ki-67). In addition, one or two non-irradiated tumors were included as control.

Statistical analysis

Survival curves of median survival and progression-free survival were compared with the log-rank (Mantel-Cox) test and Gehan-Breslow-Wilcoxon test using GraphPad Prism version 5.03. The time interval until tumors reached a size of 1000 mm^3 in the different treatment groups and the control group was compared with the two-way ANOVA. Differences in tumor growth rate between the treatment groups and the control group were compared with repeated-measures ANOVA and New-Keuls multiple comparison post analysis. A p-value below 0.05 was considered significant.

Results

^{111}In-DTPA-D2B-IRDye700DX is stable in serum and PBS

^{111}In-DTPA-D2B-IRDye700DX was stable in mouse serum and PBS directly after radiolabeling (radiochemical purity 98.7 ± 0.2 and 98.9 ± 1.4, respectively) and remained stable at 0.5 (99.1 ± 0.6 and 99.1 ± 0.4), 2.5 (99.2 ± 0.2 and 98.6 ± 0.4), 6 (98.7 ± 0.4 and 98.5 ± 0.3), and 24 h (99.6 ± 0.1 and 97.7 ± 0.9, respectively). Fluorescence intensity was set to 100% at t=0. Fluorescence intensity slowly decreased from 101.0, 94.3, and 93.4% after 0.5, 2.5, and 6h to 90.5% after 24h in PBS. In serum, fluorescence intensity was 115.8, 129.3, 122.2, and 118.2% after 0.5, 2.5, 6, and 24h.

^{111}In-DTPA-D2B-IRDye700DX specifically binds to PSMA-expressing cells

The immunoreactive fractions of ^{111}In-DTPA-D2B-IRDye700DX and ^{111}In-DTPA-D2B were 87% and 84%, respectively, which indicates that the immunoreactivity of the D2B antibody was largely preserved after the two conjugation procedures. The competitive binding assay revealed an IC_{50} of D2B of 4.0 nM (95% confidence interval: 3.0 – 5.4 nM). The IC_{50} of DTPA-D2B-IRDye700DX did not differ significantly from this value (2.1 nM, 95% confidence interval: 1.9 – 2.4 nM, $p>0.05$).

^{111}In-DTPA-D2B-IRDye700DX is gradually internalized by PSMA-expressing cells

^{111}In-DTPA-D2B-IRDye700DX and ^{111}In-DTPA-D2B gradually and specifically internalized into PSMA-expressing LS174T-PSMA cells (**Figure 1A and B**). The internalized fraction increased and reached a plateau during the first 24 h. After 48 h, 40.3 ± 2.6% and 41.6 ± 0.2% of the added activity of ^{111}In-DTPA-D2B-IRDye700DX and ^{111}In-DTPA-D2B, respectively, was internalized. Internalization of ^{111}In-DTPA-D2B-IRDye700DX and ^{111}In-DTPA-D2B was blocked by addition of an excess of unlabeled D2B, leading to an internalized fraction of 0.9 ± 0.0% and 0.9 ± 0.0%, respectively.

DTPA-D2B-IRDye700DX induces PSMA-specific tumor cell destruction upon NIR light exposure

$PSMA^+$ LS174T-PSMA cells were incubated with DTPA-D2B-IRDye700DX and irradiated with NIR light to analyze cellular toxicity of tPDT. After incubation of LS174T-PSMA cells with 10 µg/mL DTPA-D2B-IRDye700DX for 1 h, cells were irradiated at NIR radiant exposures of 2, 5, 10, 30, 50, 100, and 150 J/cm^2. To measure phototoxic cell destruction, a CellTiterGlo® luminescent cell viability assay was performed, determining the percentage of viable cells in culture based on quantitation of the ATP present, an indicator of metabolically active cells. Cellular phototoxicity occurred only in PSMA-expressing LS174T-PSMA cells incubated with DTPA-D2B-IRDye700DX and treated with NIR light. PSMA-negative LS174T-wildtype cells remained viable when treated with both conjugate and NIR light, which confirms PSMA-specificity of the therapy (104.1 ± 4.1%, 90.9 ± 4.2%, 106.2 ± 2.0%, 104.0 ± 2.3%, 100.1 ± 3.2%, 104.4 ± 3.1%, 105.5 ± 5.9%, and 111.3 ± 4.2% viable cells after NIR exposure of 0, 2, 5, 10, 30,

50, 100, and 150 J/cm^2). In PSMA-expressing tumor cells, cellular phototoxicity increased with escalating NIR light irradiation intensities. After NIR radiant exposures of 0, 2, 5, 10, 30, 50, 100, and 150 J/cm^2, 93.9 ± 2.7%, 103.5 ± 1.9%, 102.2 ± 3.6%, 99.0 ± 5.3%, 52.1 ± 1.7%, 45.0 ± 1.2%, 23.9 ± 0.9%, and 15.3 ± 1.5% of the PSMA-positive LS174T-PSMA tumor cells were viable (**Figure 1C**).

^{111}In-DTPA-D2B-IRDye700DX efficiently accumulates in PSMA-expressing tumors

^{111}In-DTPA-D2B-IRDye700DX specifically accumulated in the s.c. PSMA-positive LS174T-PSMA tumors, reaching 31.1 ± 5.0 percentage of the injected dose per gram (% ID/g) at 24 h after injection, 32.3 ± 8.2% ID/g at 48 h after injection, 33.8 ± 3.6% ID/g at 72 h after injection, and 31.7 ± 9.7% ID/g at 168 h after injection (**Figure 2A**). No significant difference in tumor uptake were observed at the different time points (one-way Anova, p=0.96). The uptake of ^{111}In-DTPA-D2B-IRDye700DX was significantly lower in all healthy tissues. Tracer accumulation in blood decreased from 6.7 ± 1.0% ID/g at 24 h p.i. to 1.9 ± 0.4% ID/g at 168 h after injection. A similar trend was observed for the kidneys, in which tracer uptake decreased from 5.5 ± 0.2% ID/g at 24 h p.i. to 1.3 ± 0.2% ID/g at 168 h after injection. Hepatic uptake ranged from 9.3 ± 2.3% ID/g at 24 h after injection to 8.1 ± 1.4% ID/g at 168 h after injection, uptake in the spleen reached a maximum of 8.9 ± 0.6% ID/g at 24 h after injection. Pre-operatively performed μSPECT/CT and NIRF imaging was performed 24, 48, 72, and 168 h p.i. and tumors were clearly visualized with both modalities for all time points. Representative images acquired at 24 h p.i. are displayed in **Figure 2B**. Intra-operative NIRF imaging could be used for guided resection of the tumors.

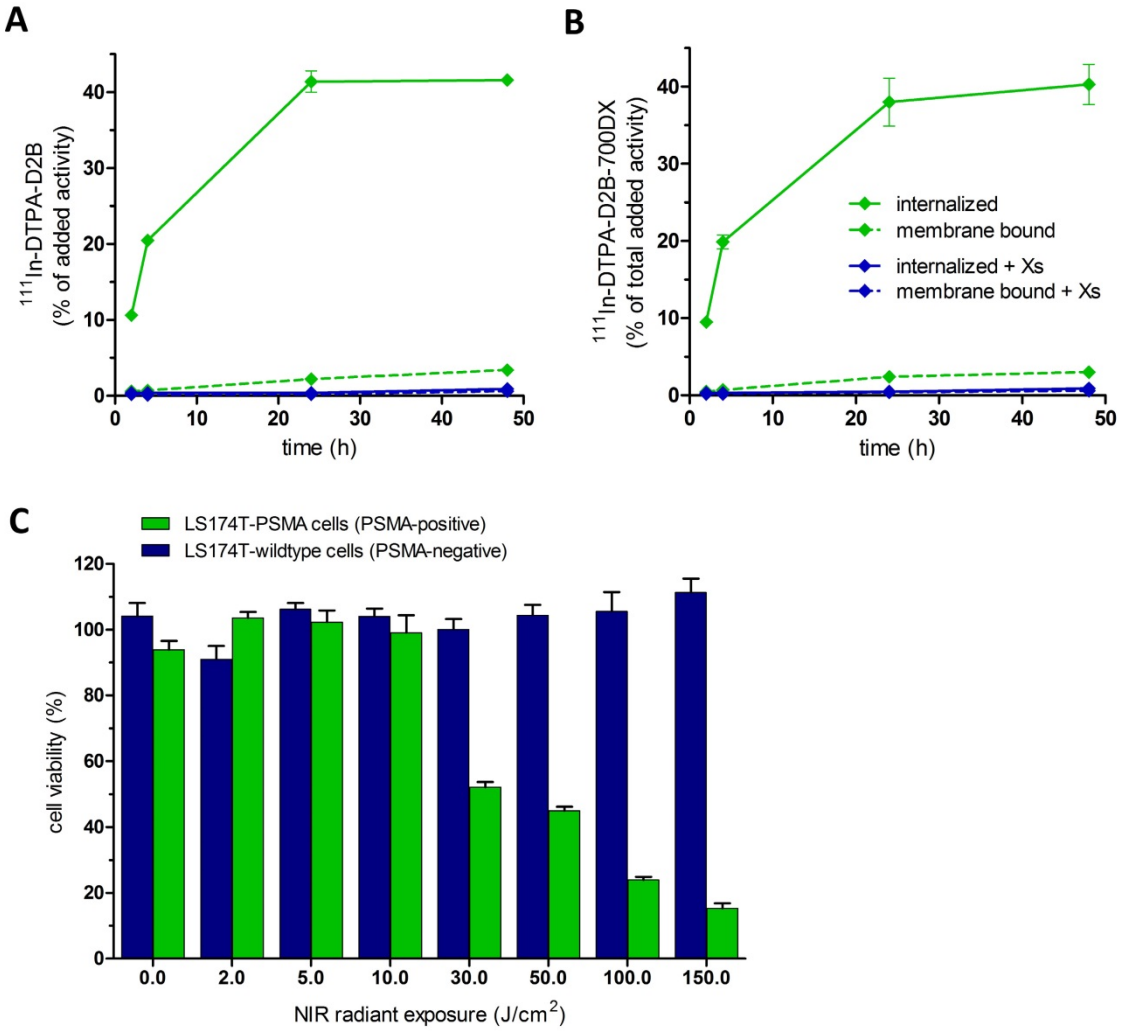

Figure 1: Internalization kinetics of ^{111}In-DTPA-D2B (A) and ^{111}In-DTPA-D2B-IRDye700DX (B) in LS174T-PSMA cells. Binding and internalization is presented as the percentage of the added activity (mean ± SD). C) Cell viability of LS174T-PSMA cells in vitro following incubation with 10 μg/mL DTPA-D2B-IRDye700DX and NIR light irradiation with radiant exposures of 2, 5, 10, 30, 50, 100, and 150 J/cm^2.

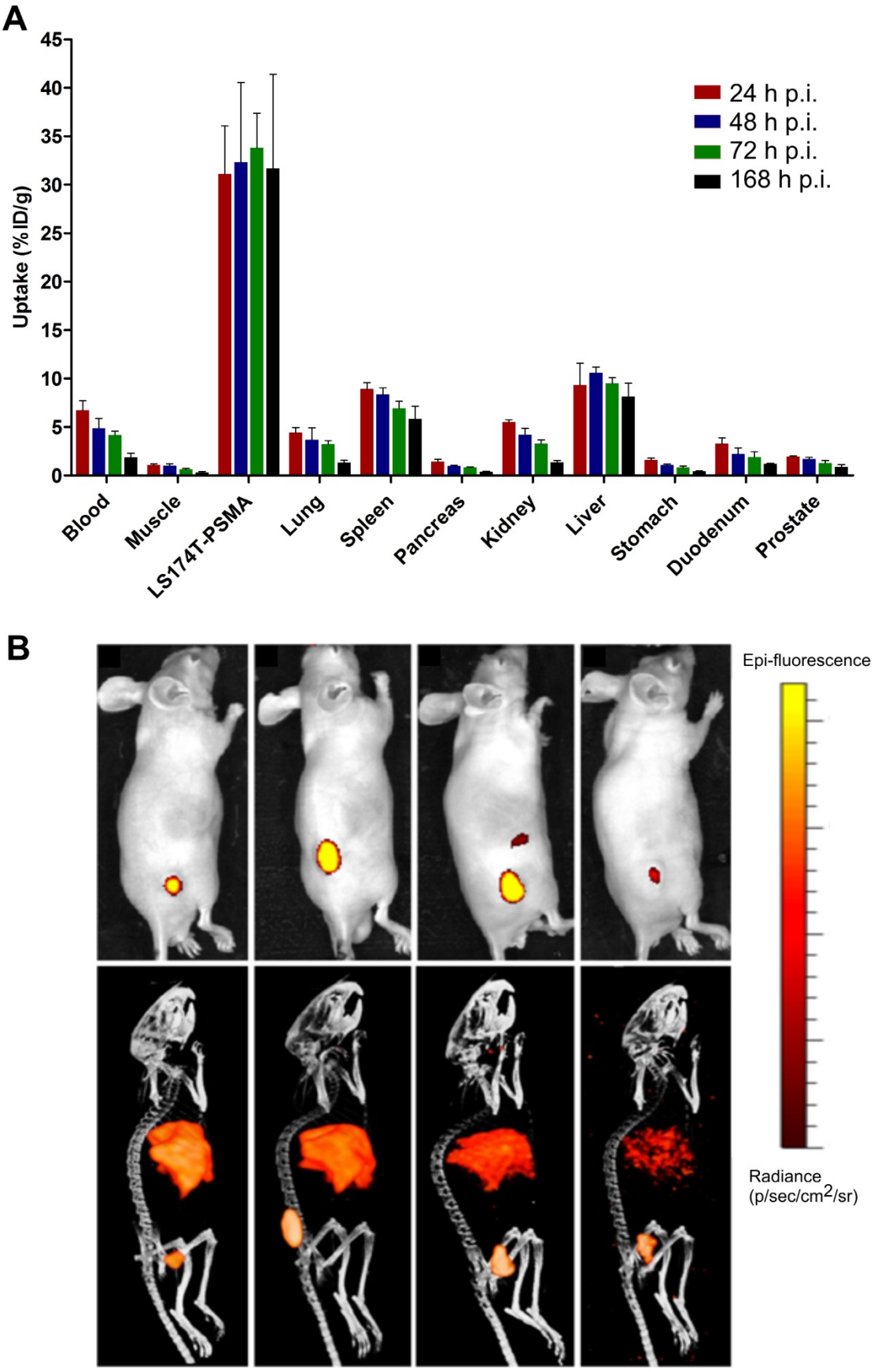

Figure 2: A) Biodistribution of ^{111}In-DTPA-D2B-IRDye700DX (30 µg and 8 MBq per mouse, n=5 per group) in the PSMA-expressing tumors and several healthy tissues. B) NIRF (top) and µSPECT/CT (bottom) in mice (different mice per time point were used) with s.c. LS174T-PSMA tumors at 24, 48, 72, and 168h after injection of 30 µg of ^{111}In-DTPA-D2B-IRDye700DX.

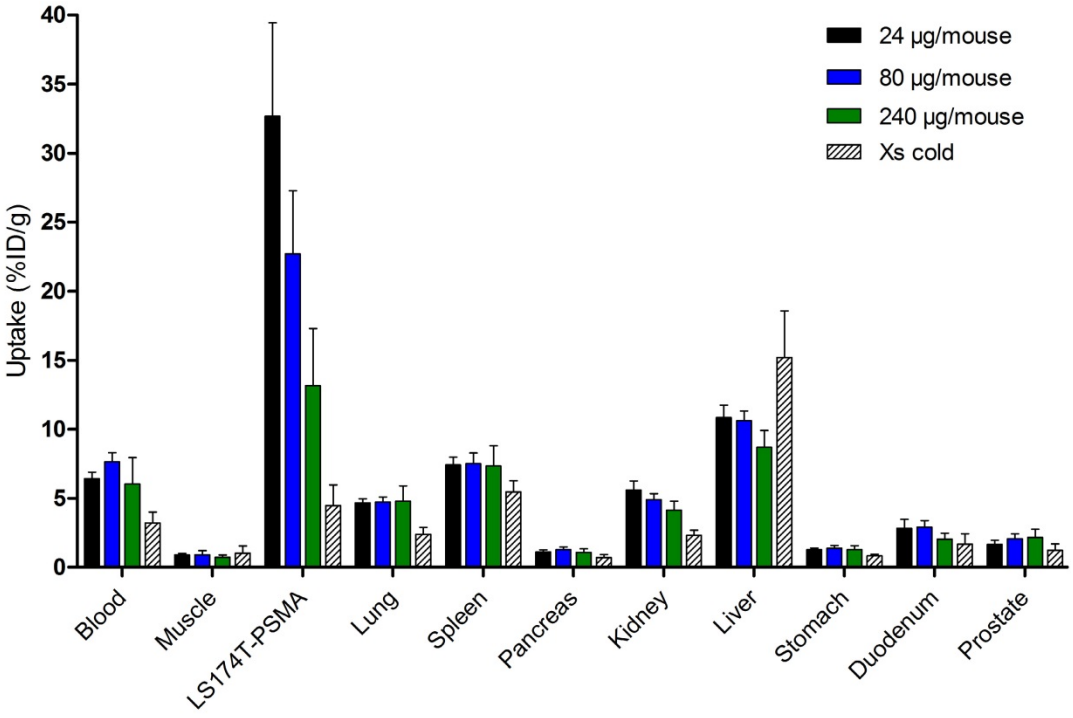

Figure 3: Biodistribution of different doses of ^{111}In-DTPA-D2B-IRDye700DX (24, 80, or 240 µg/mouse, 8 MBq/mouse, n=5 mice per group) at 24 h after injection. One group of mice received 300 µg of D2B i.v. 2 days prior to i.v. application of 24 µg of ^{111}In-DTPA-D2B-IRDye700DX to block the uptake (Xs cold condition).

As no significant difference in tumor uptake at the different time points was observed, the dose-finding study was analyzed at 24 h p.i. to minimize the chance of degradation of the dual-labeled tracer *in vivo* when NIR light irradiation will be performed. Highest tumor uptake (% ID/g) was observed for a conjugate dose of 24 µg/mouse, reaching 32.7 ± 6.8% ID/g. For conjugate doses of 80 and 240 µg/mouse, tumor uptake decreased to 22.7 ± 4.6 and 13.2 ± 4.1% ID/g, respectively (**Figure 3**). A similar trend was observed for hepatic uptake, decreasing from 10.8 ± 0.9% ID/g at a dose of 24 µg/mouse to 10.6 ± 0.7% ID/g and 8.7 ± 1.2% ID/g for 80 and 240 µg/mouse, respectively.

PDT using DTPA-D2B-IRDye700DX inhibits tumor growth and significantly improves survival

In the PDT therapy experiment in xenografted mice, several treatment conditions were tested. One group of 7 mice with s.c. PSMA$^+$ LS174T-PSMA tumors was included that received NIR light irradiation once, at 24 h p.i. at an intensity of 150 J/cm^2. In addition, 3 groups of mice were included that received 3 NIR light exposures (at 24, 48, and 72 h after injection of the conjugate) at intensities of 50, 100, or 150 J/cm^2. Moreover, one control group was included which did not receive the conjugate, but was irradiated with NIR light and one control group was included which received neither the conjugate nor NIR light irradiation. Mean tumor sizes at the day of NIR treatment were 91.9 ± 32.6 mm^3 (group: 1x 150 J/cm^2), 28.6 ± 21.7 mm^3 (group: 3x 150 J/cm^2), 33.3 ± 33.7 mm^3 (group: 3x 100 J/cm^2), 29.6 ± 37.2 mm^3 (group: 3x 50 J/cm^2). Tumor sizes in the 1x 150 J/cm^2 group were significantly higher compared to the other groups ($p<0.05$).

Mean tumor size in the control group that was irradiated but did not receive the conjugate was 31.7 ± 35.3 mm^3 and in the group that received neither conjugate nor NIR light exposure was 45.5 ± 21.7 mm^3.

Tumor growth after treatment with 1x 150 J/cm^2 as well as with 3x 50, 100, or 150 J/cm^2 in individual mice is depicted in **Figure 4**. Analysis of survival (until tumors reached a size of 1,000 mm^3 or until humane endpoints were reached) revealed significantly longer overall survival in mice that received 80 µg of the conjugate followed by a single NIR light exposure at 24h post injection at a NIR light exposure of 150 J/cm^2 (median survival 73 days) compared to mice that neither received the conjugate nor received NIR light exposure (median survival 16 days) and mice that received NIR light exposure only (median survival 16 days) ($p=0.0453$) (**Figure 4A**). In addition, progression-free survival was significantly prolonged in mice treated with 80 µg of the conjugate followed by NIR light of 1x 150 J/cm^2 (progression-free survival 61 days) as compared to both control groups (progression-free survival of 2 and 1 days, respectively) ($p=0.0229$) (**Figure 4B**).

However, three out of seven mice out of the treatment group died three days after NIR light exposure (these mice were excluded from further analysis). Upon necropsy/autopsy, no signs of skin/tissue/organ damage due to treatment were found. All remaining four mice out of the treatment group developed eschars at the tumor side within 2 days after NIR light exposure, which healed within 7-14 days and resulted in the formation of a scar. None of the mice out of the two control groups developed eschars and subsequent scars.

To evaluate whether fractionated NIR light exposures increase the therapeutic efficacy, groups of mice were included which received NIR light irradiation of 50, 100, or 150 J/cm² at 24, 48, and 72 h after i.v. administration of 80 µg of the conjugate. Compared to the control groups, NIR irradiation regimens of 3x 50 and 3x 100 J/cm² significantly increased progression-free and overall survival (p=0.0029) (**Figure 4A and B**). Progression-free survival (9.5 and 15 days, respectively, p=0.1606) and overall survival (32 and 36 days, respectively, p=0.5566) were not significantly different between mice treated with 3x 50 and 3x 100 J/cm². Compared to a single NIR light exposure of 150 J/cm², progression-free survival upon fractionated NIR light exposure of 3x 50 (p=0.0039) and 3x 100 (p=0.0148) J/cm² was significantly reduced (**Figure 4B**). For overall survival similar observations were made; single treatment with 150 J/cm² of NIR light resulted in significantly prolonged overall survival compared to fractionated treatment with 3x 100 J/cm² of NIR light (p=0.0294). None of the mice treated with 3x 50 J/cm² developed eschars/scars after NIR light exposure.

Compared to mice treated with 1x 150 J/cm², progression-free and overall survival were not significantly different between mice treated with 3x 150 J/cm² (p=0.8644). Six out of 7 mice (86%) treated with 3x 150 J/cm² developed eschars/scars after NIR light exposure.

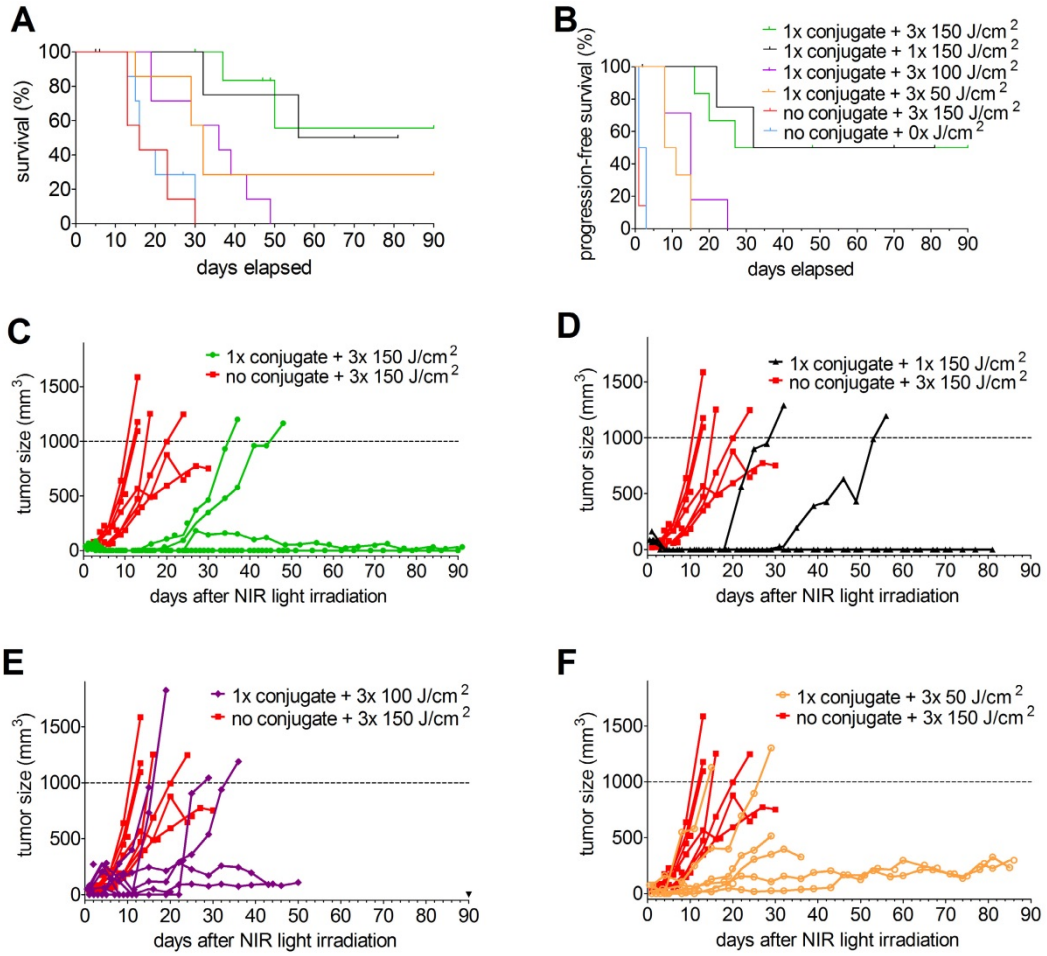

Figure 4: Kaplan-Meier plots of overall (A) and progression-free survival (B) (7 mice/group, excluded mice are indicated with apostrophes in the graphs) and tumor growth (C-F) of male BALB/c nude mice with s.c. PSMA⁺ LS174T-PSMA tumors after i.v. injection of 80 µg of DTPA-D2B-IRDye700DX, followed by exposure to different NIR light irradiation regimens. In panel C-F, tumor growth in mice that did not receive the conjugate but where irradiated with the highest NIR light dose (3x 150 J/cm²) (control group), was compared to that in mice treated with a single administration of the conjugate followed by NIR light exposure of 3x 150 J/cm² (C), 1x 150 J/cm² (D), 3x 100 J/cm² (E), and 3x 50 J/cm² (F).

To ensure that DTPA-D2B-IRDye700DX itself (without NIR light exposure) has no therapeutic effect either, overall survival was evaluated in mice treated with the conjugate only and compared to that of mice treated with neither conjugate nor light and to mice that received NIR light only (without prior conjugate administration) in a subsequent experiment. Overall survival between these groups was not significantly different (12, 13, and 14 days, respectively, p=0.5902). In this experiment, therapeutic efficacy was also tested in mice with s.c. PSMA-negative LS174T-wildtype tumors which received 80 µg of the conjugate followed by NIR light exposure (1x 100 J/cm²) at 24h p.i.. Compared to the three control groups, overall survival (21 days) was significantly prolonged (p=0.0283).

To evaluate therapy-induced changes in the tumors, LS174T-PSMA tumors treated with 80 µg of DTPA-D2B-IRDye700DX and harvested 1 or 24 h after NIR light irradiation (150 J/cm²), and untreated control tumors were analyzed immunohistochemically (**Figure 5**).

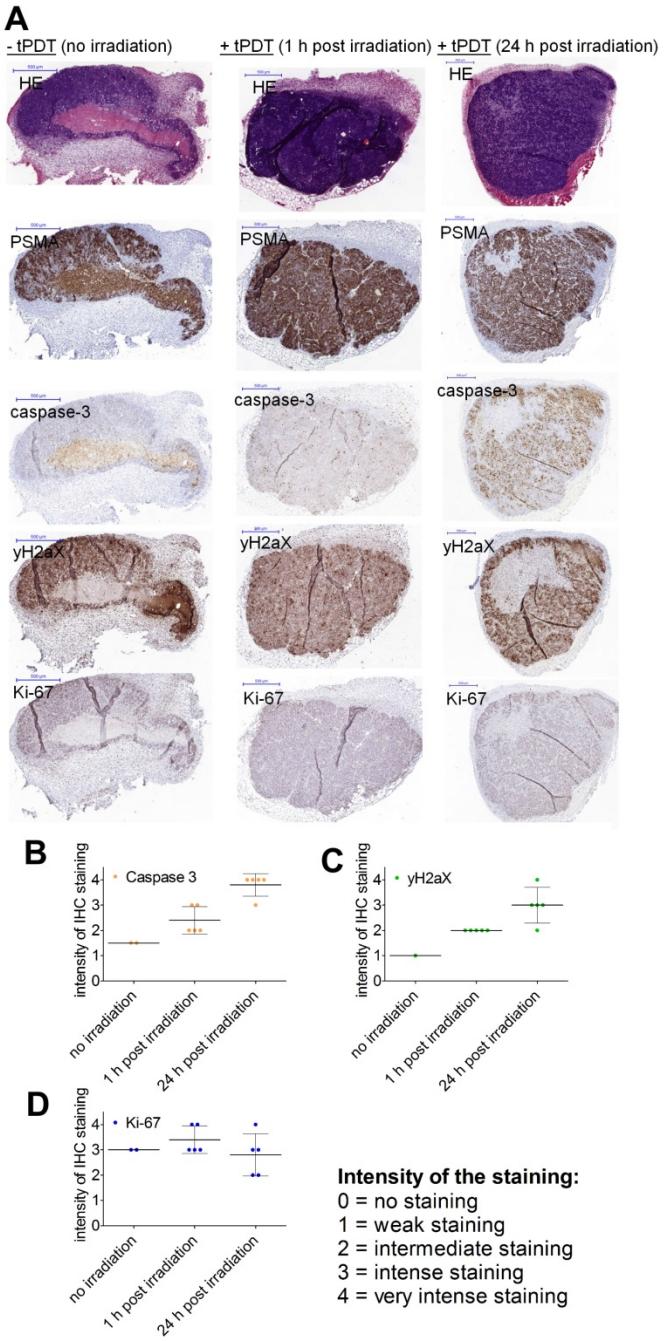

Figure 5: A) HE, PSMA, caspase-3, γH2aX, and Ki-67 stainings of s.c. PSMA+ LS174T-PSMA tumors after i.v. administration of PBS (left) or 80 µg of ^{111}In-DTPA-D2B-IRDye700DX (middle (tumors dissected 1h after tPDT) and right (tumors dissected 24h after tPDT)). All scale bars indicate 500 µm. B) Staining intensity of immunohistochemical stainings of treated (n=5) and non-treated tumor.

Categorization of the immunohistochemical stainings revealed that treated tumor sections showed higher expression of caspase-3 and γH2AX compared to non-treated tumors. Caspase-3 and γH2AX expression were higher in tumors resected at 24 h after NIR light exposure compared to 1 h post irradiation. Ki-67 stainings were performed to show viability of the tumor sections.

PDT using DTPA-D2B-IRDye700DX does not induce nephro- or hepatotoxicity

To evaluate potential nephro- and hepatotoxcity of PSMA-tPDT, blood samples were obtained prior to any treatment from treated and non-treated mice (with conjugate and without NIR exposure, without conjugate and with NIR exposure, and with both conjugate and NIR light on mice with PSMA-negative tumors) 1 week after treatment. No significant changes in aspartate/alanine transaminase (AST/ALT) were observed between the treatment groups before and after therapy ($p=0.0660$ for ALT and $p=0.1311$ for AST). Creatinine levels were significantly increased in the treatment group at 1 week after therapy compared to baseline levels ($p=0.001$), however, this elevation in creatinine levels was reversible and creatinine levels measured directly after euthanasia in these mice were restored.

Discussion

Despite improvements in PCa oncological surgery (biochemical) recurrences frequently occur, which may be attributed to two major issues: first, the translation from pre-operatively obtained images to the surgical field can be extremely challenging for surgeons, particularly in the abdominal region. Thus, some lesions may not be removed and may cause disease recurrence. Second, wide local excision of tumors may be restricted due to close proximity of the rectum, sphincter and erectile nerves and lead to incomplete surgical removal. To address both issues, in this study a multimodal anti-PSMA targeting agent for highly specific pre- and intra-operative tumor localization, surgical guidance, and PSMA-targeted tumor cell destruction using tPDT was characterized *in vivo*.

So far, several approaches for antibody-targeted PDT have been developed. Mangadlao et al. used the phthalocyanine-based photosensitizer Pc4 in a preclinical study investigating the potential of PSMA-targeted gold nanoparticles containing Pc4 as imaging and PDT agent [28]. In the majority of these studies, the phthalocyanine IRDye700DX was used as a photosensitizer, as it absorbs light in the near-infrared (NIR) range, which allows deeper tissue penetration compared to visible light. In addition, IRDye700DX can be covalently conjugated to targeting molecules using its NHS ester. Moreover, IRDye700DX has a higher extinction coefficient ($2.1x10^5$ $M^{-1}cm^{-1}$ at 689 nm) than non-NIR photosensitizers [8]. This might be advantageous, as low extinction coefficients require conjugation of large numbers of photosensitizers to a targeting molecule, which might decrease the binding affinity and/or the tumor targeting characteristics of the targeting vehicle [29]. However, efficacy of photodynamic therapy may also dependent upon singlet oxygen quantum yield. Photosensitizers with higher singlet oxygen quantum yields are generally more effective in generating reactive singlet oxygen species.

In the present study, ^{111}In-DTPA-D2B-IRDye700DX was shown to be stable in serum and PBS, and it specifically binds to and is gradually internalized by PSMA-expressing cells. Binding and internalization capacity were similar to unconjugated D2B [19, 27]. *In vitro*, we demonstrated that DTPA-D2B-IRDye700DX induced PSMA-specific tumor cell destruction upon NIR light exposure. *In vivo*, ^{111}In-DTPA-D2B-IRDye700DX efficiently accumulated in PSMA-expressing tumors. Ex vivo biodistribution studies also revealed tracer accumulation in the liver and spleen, which may be attributed to relative lipophilicity of IRDye700DX. To avoid major changes in biodistribution and accumulation in liver and spleen, the molar substitution ratio of IRDye700DX to antibody was limited to 3.3 : 1, which allowed NIRF imaging and tPDT in the tumor. Biodistribution was determined at different time points to identify the time point with the highest tumor accumulation, which was assumed the optimal time point for NIR light irradiation. As no significant difference in tumor accumulation was observed between the different time points after injection, the earliest time point (24 h p.i.), in line with previous studies [8], was selected for subsequent *in vivo* studies for two reasons: first, in clinical settings, it is more practical to perform imaging/therapy early after injection. Second, at later time points after injection, degradation of the antibody-IRDye700DX conjugate might occur by either breakdown in the liver or in the tumor after internalization. In the present study, at 24 h after administration PSMA-expressing tumors were clearly visualized on pre-operative μSPECT/CT and intra-operative NIRF images, which could also be used for image-guided resection of the tumors.

In a biodistribution experiment, three different tracer doses were evaluated. In theory, anti-tumor efficacy of tPDT should increase with higher amounts of photosensitizer in the tumor, which can be reached by escalating the tracer dose. Mitsunaga et al. showed

that anti-tumor efficacy using 300 µg the anti-EGFR mAb panitumumab conjugated to IRDye700DX was higher compared to 50 µg [8]. However, at a certain dose, saturation of the epitopes in the tumor will occur, leading to non-specific localization and high amounts of photosensitizer in surrounding tissues. Indeed, Mitsunaga and colleagues observed higher background levels in mice administered with 300 µg instead of 50 µg of the conjugate [8]. To minimize non-specific accumulation in tumor and other organs but still be able to reach sufficient therapy efficacy, we selected the tracer dose of 80 µg for tPDT studies.

In previous studies, the radiant exposure of NIR light applied to tumors typically ranged between 30 and 100 J/cm² [8, 30, 31]. In the present study, efficacy of single and multiple administrations of low and high radiant exposures were evaluated (50, 100, or 150 J/cm²). NIR light irradiation with all three radiant exposures caused significant prolongation of progression-free survival from 1-2 to 61 days and overall survival from 16 to 73 days compared to non-treated control tumors. Chen et al. performed PSMA-tPDT using the low-molecular-weight theranostic photosensitizer, YC-9, which was synthesized by conjugating IRDye700DX with a PSMA targeting Lys-Glu-urea [32]. YC-9 was applied four times within 48 h followed by NIR light exposure of 100 J/cm² at 4h p.i.. The authors report a prolongation of overall survival of mice with s.c. PSMA-expressing tumors from 24-30 to 57 days upon exposure to 100 J/cm² of NIR light [32]. In the present study, the effect of repeated, fractionated NIR light exposure was evaluated. As antibody molecules circulate longer compared to small molecules, the conjugate was applied only once in the present study. While multiple fractionated NIR light exposures resulted in prolonged progression-free and overall survival compared to control groups, single administration of 150 J/cm² caused the most significant benefit for progression-free and overall survival, which was similar to administration of 3x 150 J/cm². However, the majority of mice treated with these high NIR light doses developed side-effects (eschar and scar formation), while side-effects were less prominent and frequent in mice treated with lower doses. Okuyama and colleagues have shown that skin damage after NIR light exposure may be attributed to heat developed by the LED system [33].

As biodistribution revealed high liver/spleen uptake, hepatotoxicity was evaluated in the present study. However, no hepatotoxicity was observed. In addition, as NIR light irradiation can be applied locally, liver and spleen uptake are not expected to cause side effects of the therapy. Observed nephrotoxicity was mild and reversible in this study and may be due to reduced fluid intake of treated mice directly after the procedure and increased fluid metabolism due to healing processes.

Compared to the three control groups, overall survival was significantly prolonged in the PSMA-negative control tumors. One explanation for this may be nonspecific localization of the conjugate in the tumor due to the EPR (enhanced permeability and retention) effect.

To illustrate therapy-induced changes in the tumors, immunohistochemical assessments were performed on LS174T-PSMA tumors harvested 1 or 24 h after NIR light irradiation, as well as on untreated control tumors. Compared to controls, expression of γH2AX and caspase-3 were significantly higher in treated tumor sections, suggesting the induction of DNA double strand breaks and apoptosis following treatment. Although these observations need to be investigated further in a larger study, these data support the observed changes in tumor growth. One limitation of this study is that no isotype control for the antibody was used, so potential contributions of inflammatory uptake through FcR interactions cannot be discriminated from specific epithelial binding.

Here, we have shown feasibility of ^{111}In-DTPA-D2B-IRDye700DX for pre- and intra-operative detection of PSMA$^+$ tumors with radionuclide and NIR fluorescence imaging and PSMA-targeted PDT in a transfected tumor model which stably expresses PSMA. In the next step, this approach will be evaluated in prostate cancer cell lines that naturally express PSMA.

In the clinical setting, this tPDT approach could be embedded into a multimodal approach in which the theranostic targeting agent could be used for pre-operative visualization of tumor lesions to evaluate the tumor load and the localization of the tumor lesions. In addition, the targeting molecule could be used during surgery for guidance to deeper-seeded tumor lesions using a gamma probe. Once these lesions have been brought to the surface, the fluorescent signal of the multimodal targeting agent can be used to visually guide the surgeon towards precise resection of the lesions. Finally, in areas where wide local excision is precluded, the targeting agent could be used for PSMA-tPDT to destroy residual tumor tissue that could not be removed surgically. The elimination of these PSMA$^+$ residual tumor cells is crucial as patients with PSMA-expressing tumors show an increased rate of biochemical recurrence [34] and the well-established role of PSMA in the aggressiveness of malignant cells [35].

Conclusion

In the present study, the development of the theranostic multimodal agent ^{111}In-DTPA-D2B-IRDye700DX was described and optimized *in vitro* and *in vivo* in a mouse model to improve management of PCa. It was demonstrated that ^{111}In-DTPA-D2B-IRDye700DX can be used for pre-operative visualization of tumors using μSPECT/CT and for intra-operative tumor localization using NIRF imaging. Moreover, NIRF imaging can be used to guide surgical removal where possible and/or guide (additional) PSMA-tPDT in areas where tumor remnants cannot be removed surgically due to their proximity to important surrounding structures such as nerves innervating the urinary bladder or erectile functions. It was demonstrated that PSMA-tPDT can efficiently inhibit growth of PSMA-expressing tumors and significantly prolong median survival.

These preclinical findings encourage future clinical studies with radiolabeled targeting molecules conjugated to IRDye700DX to improve diagnostic imaging, provide surgical guidance, and enable tPDT of non-resectable tumor remnants.

Acknowledgements

The authors thank Bianca Lemmers-van de Weem, Iris Lamers-Elemans, Mike Peters and Kitty Lemmens-Hermans for technical assistance with the animal experiments.

Competing Interests

The authors have declared that no competing interest exists.

References

1. Siegel RL, Miller KD, Jemal A. Cancer statistics, 2016. CA Cancer J Clin. 2016; 66: 7-30.
2. Heidenreich A, Bastian PJ, Bellmunt J, Bolla M, Joniau S, van der Kwast T, et al. EAU guidelines on prostate cancer. Part II: Treatment of advanced, relapsing, and castration-resistant prostate cancer. Eur Urol. 2014; 65: 467-79.
3. Briganti A, Larcher A, Abdollah F, Capitanio U, Gallina A, Suardi N, et al. Updated nomogram predicting lymph node invasion in patients with prostate cancer undergoing extended pelvic lymph node dissection: the essential importance of percentage of positive cores. Eur Urol. 2012; 61: 480-7.
4. Eastham JA, Kuroiwa K, Ohori M, Serio AM, Gorbonos A, Maru N, et al. Prognostic significance of location of positive margins in radical prostatectomy specimens. Urology. 2007; 70: 965-9.
5. Eastham JA, Kattan MW, Riedel E, Begg CB, Wheeler TM, Gerigk C, et al. Variations among individual surgeons in the rate of positive surgical margins in radical prostatectomy specimens. J Urol. 2003; 170: 2292-5.
6. Yossepowitch O, Briganti A, Eastham JA, Epstein J, Graefen M, Montironi R, et al. Positive surgical margins after radical prostatectomy: a systematic review and contemporary update. Eur Urol. 2014; 65: 303-13.
7. Agostinis P, Berg K, Cengel KA, Foster TH, Girotti AW, Gollnick SO, et al. Photodynamic therapy of cancer: an update. CA Cancer J Clin. 2011; 61: 250-81.
8. Mitsunaga M, Ogawa M, Kosaka N, Rosenblum LT, Choyke PL, Kobayashi H. Cancer cell-selective *in vivo* near infrared photoimmunotherapy targeting specific membrane molecules. Nat Med. 2011; 17: 1685-91.
9. Israeli RS, Powell CT, Fair WR, Heston WD. Molecular cloning of a complementary DNA encoding a prostate-specific membrane antigen. Cancer Res. 1993; 53: 227-30.
10. Minner S, Wittmer C, Graefen M, Salomon G, Steuber T, Haese A, et al. High level PSMA expression is associated with early PSA recurrence in surgically treated prostate cancer. Prostate. 2011; 71: 281-8.
11. Rybalov M, Ananias HJ, Hoving HD, van der Poel HG, Rosati S, de Jong IJ. PSMA, EpCAM, VEGF and GRPR as imaging targets in locally recurrent prostate cancer after radiotherapy. Int J Mol Sci. 2014; 15: 6046-61.
12. Ananias HJ, van den Heuvel MC, Helfrich W, de Jong IJ. Expression of the gastrin-releasing peptide receptor, the prostate stem cell antigen and the prostate-specific membrane antigen in lymph node and bone metastases of prostate cancer. Prostate. 2009; 69: 1101-8.
13. Silver DA, Pellicer I, Fair WR, Heston WD, Cordon-Cardo C. Prostate-specific membrane antigen expression in normal and malignant human tissues. Clin Cancer Res. 1997; 3: 81-5.
14. Kawakami M, Nakayama J. Enhanced expression of prostate-specific membrane antigen gene in prostate cancer as revealed by in situ hybridization. Cancer Res. 1997; 57: 2321-4.
15. Bostwick DG, Pacelli A, Blute M, Roche P, Murphy GP. Prostate specific membrane antigen expression in prostatic intraepithelial neoplasia and adenocarcinoma: a study of 184 cases. Cancer. 1998; 82: 2256-61.
16. Graham K, Lesche R, Gromov AV, Bohnke N, Schafer M, Hassfeld J, et al. Radiofluorinated derivatives of 2-(phosphonomethyl)pentanedioic acid as inhibitors of prostate specific membrane antigen (PSMA) for the imaging of prostate cancer. J Med Chem. 2012; 55: 9510-20.
17. Troyer JK, Beckett ML, Wright GL, Jr. Detection and characterization of the prostate-specific membrane antigen (PSMA) in tissue extracts and body fluids. Internat J Cancer. 1995; 62: 552-8.
18. Lutje S, Rijpkema M, Helfrich W, Oyen WJ, Boerman OC. Targeted radionuclide and fluorescence dual-modality imaging of cancer: preclinical advances and clinical translation. Mol Imaging Biol. 2014; 16: 747-55.
19. Lutje S, van Rij CM, Franssen GM, Fracasso G, Helfrich W, Eek A, et al. Targeting human prostate cancer with 111In-labeled D2B IgG, F(ab')2 and Fab fragments in nude mice with PSMA-expressing xenografts. Contrast Media Mol Imaging. 2015; 10: 28-36.
20. Lutje S, Rijpkema M, Franssen GM, Fracasso G, Helfrich W, Eek A, et al. Dual-Modality Image-Guided Surgery of Prostate Cancer with a Radiolabeled Fluorescent Anti-PSMA Monoclonal Antibody. J Nucl Med. 2014; 55: 995-1001.
21. Rijpkema M, Bos DL, Cornelissen AS, Franssen GM, Goldenberg DM, Oyen WJ, et al. Optimization of Dual-Labeled Antibodies for Targeted Intraoperative Imaging of Tumors. Mol Imaging. 2015; 14: 348-55.
22. Lindmo T, Bunn PA, Jr. Determination of the true immunoreactive fraction of monoclonal antibodies after radiolabeling. Methods Enzymol. 1986; 121: 678-91.
23. Heskamp S, Laverman P, Rosik D, Boschetti F, van der Graaf WTA, Oyen WJG, et al. Imaging of Human Epidermal Growth Factor Receptor Type 2 Expression with F-18-Labeled Affibody Molecule Z(HER2:2395) in a Mouse Model for Ovarian Cancer. J Nucl Med. 2012; 53: 146-53.
24. de Boer E, Warram JM, Hartmans E, Bremer PJ, Bijl B, Crane LM, et al. A standardized light-emitting diode device for photoimmunotherapy. J Nucl Med. 2014; 55: 1893-8.
25. Shirasu N, Yamada H, Shibaguchi H, Kuroki M, Kuroki M. Potent and specific antitumor effect of CEA-targeted photoimmunotherapy. Int J Cancer. 2014; 135: 2697-710.
26. Lutje S, Rijpkema M, Goldenberg DM, van Rij CM, Sharkey RM, McBride WJ, et al. Pretargeted dual-modality immuno-SPECT and near-infrared fluorescence imaging for image-guided surgery of prostate cancer. Cancer Res. 2014; 74: 6216-23.
27. Lutje S, Gerrits D, Molkenboer-Kuenen JD, Herrmann K, Fracasso G, Colombatti M, et al. Characterization of site-specifically conjugated monomethyl auristatin E- and duocarmycin-based anti-PSMA antibody-drug conjugates for treatment of PSMA-expressing tumors. J Nucl Med. 2017; 59: 494-501.
28. Mangadlao JD, Wang X, McCleese C, Escamilla M, Ramamurthy G, Wang Z, et al. Prostate-Specific Membrane Antigen Targeted Gold Nanoparticles for Theranostics of Prostate Cancer. ACS Nano. 2018; 12: 3714-25.
29. Mitsunaga M, Nakajima T, Sano K, Choyke PL, Kobayashi H. Near-infrared theranostic photoimmunotherapy (PIT): repeated exposure of light enhances the effect of immunoconjugate. Bioconjug Chem. 2012; 23: 604-9.
30. Watanabe R, Hanaoka H, Sato K, Nagaya T, Harada T, Mitsunaga M, et al. Photoimmunotherapy targeting prostate-specific membrane antigen: are antibody fragments as effective as antibodies? J Nucl Med. 2015; 56: 140-4.
31. Sato K, Watanabe R, Hanaoka H, Harada T, Nakajima T, Kim I, et al. Photoimmunotherapy: comparative effectiveness of two monoclonal antibodies targeting the epidermal growth factor receptor. Mol Oncol. 2014; 8: 620-32.
32. Chen Y, Chatterjee S, Lisok A, Minn I, Pullambhatla M, Wharram B, et al. A PSMA-targeted theranostic agent for photodynamic therapy. J Photochem Photobiol B. 2017; 167: 111-6.
33. Okuyama S, Nagaya T, Ogata F, Maruoka Y, Sato K, Nakamura Y, et al. Avoiding thermal injury during near- infrared photoimmunotherapy (NIR-PIT): the importance of NIR light power density. Oncotarget. 2017; 8: 113194-201.
34. Ross JS, Sheehan CE, Fisher HAG, Kaufman RP, Kaur P, Gray K, et al. Correlation of primary tumor prostate-specific membrane antigen expression with disease recurrence in prostate cancer. Clin Cancer Res. 2003; 9: 6357-62.

35. Perico ME, Grasso S, Brunelli M, Martignoni G, Munari E, Moiso E, et al. Prostate-specific membrane antigen (PSMA) assembles a macromolecular complex regulating growth and survival of prostate cancer cells *in vitro* and correlating with progression *in vivo*. Oncotarget. 2016; 7: 74189-202.